Journal of Sound and Vibration (1997) **200**(4), 419–431

NON-LINEAR VIBRATION OF POWER TRANSMISSION BELTS

J. Moon and J. A. Wickert

Department of Mechanical Engineering, Carnegie Mellon University, Pittsburgh, PA 15213, *U.S.A.*

(*Received* 29 *January* 1996, *and in final form* 22 *July* 1996)

Non-linear vibration of a prototypical power transmission belt system, which is excited by pulleys having slight eccentricity, is investigated through experimental and analytical methods. Laboratory measurements demonstrate the role of non-linearity in setting the belt's response, particularly in the near-resonance region, and at high running speeds. The belt is coated with a retroreflective medium so as to improve displacement and velocity measurements made through non-contact laser interferometry. A frequency crossing diagram relates the belt's speed-dependent excitation and natural frequencies, and is shown to be useful for identifying those speeds at which resonance is expected. Distinctive jump and hysteresis phenomena in the near-resonant response are observed experimentally, and are also studied with a model that includes non-linear stretching of the belt. In that regard, a modal perturbation solution is developed in the context of the asymptotic method of Krylov, Bogoliubov, and Mitropolsky for a general, continuous, non-autonomous, gyroscopic system with weakly non-linear stiffness. The solution is subsequently specialized to the belt vibration problem at hand. Near- and exact-resonant response amplitudes are predicted by the perturbation method, and they are compared with those obtained by laboratory tests and by direct numerical simulation of the non-linear model.

1. INTRODUCTION

Continuous belts are used to transmit power and motion, and they frequently replace such comparatively more expensive and complicated drive train components as gears or linkages. Since belts are also relatively flexible, they can play an important role in absorbing shock loads. On the other hand, the additional compliance renders belts more susceptible to large amplitude vibration and squeal noise problems [1–3], motivating the problem at hand.

Power transmission components are inherently coupled, and their mutual interactions contribute to drive train vibration and resonance. Common excitation sources include slightly-eccentric drive or idle pulleys and sprockets, material inhomogeneity, polygonal action at the interface of meshing teeth and sprockets, and edge loading. Pulley and belt systems can also be excited parametrically by tension variations, either directly [4] or through variations in one span of the belt which are preserved during contact with a pulley, only to be later relieved as the belt disengages from it [5]. In practice, belt resonances are avoided either by drive train redesign or through the addition of tensioners and dampers [6].

Previous mathematical treatments of belt vibration have concentrated on the problems of linear response and dynamic stability. At an early stage of the problem's understanding, Mahalingam [7] examined forced vibration of power transmission chains, concentrating on the excitation associated with the geometric irregularity of the chain-to-sprocket

0022–460X/97/090419 + 13 $25·00/0/sv960709

interface. More recently, Asokanthan and Ariaratnam [8], and Wang [9], have studied parametric instabilities in belt and chain systems and the periodic tension fluctuations which are caused by the impulsive forces generated during chain-to-sprocket impact.

The present paper concentrates on the non-linear vibration of a prototypal power transmission belt model, and on such experimentally-observed behavior as multi-valued response amplitudes and irreversible near-resonant amplitude jumps. Following laboratory experiments, the non-linear equations of motion and boundary conditions of the belt model are cast in a standard form for distributed-parameter gyroscopic systems. Extending previous developments for weakly non-linear autonomous systems, an averaging solution is developed through the asymptotic method of Krylov, Bogoliubov, and Mitropolsky for the response in both the near- and exact-resonance regions. Closed form expressions for the vibration amplitude and phase are derived, and the method is applied in several illustrative examples.

2. BELT RESPONSE MEASUREMENTS

In order to guide subsequent modelling, laboratory measurements were first conducted with the high speed belt stand illustrated in Figure 1. The seamless timing belt with span $L = 860$ mm was driven by a variable speed motor over drive and idle pulleys of common pitch radius $r = 63$ mm. The idle pulley was mounted on rotation and translation stages so as to minimize through cut-and-try adjustment those excitation sources associated with pulley misalignment.

Transverse vibration of the belt was measured by using a Michelson-style laser interferometer. Fiber optic leads were used to establish the paths for the reference and target light beams. The interferometer measured changes in these two light path lengths through the interference fringes generated by superposition of coherent beams that reflected from (1) a stationary reference surface and (2) a moving target, namely, the belt itself. To ensure that sufficient light was scattered from the belt and into the optical head, the belt was coated with a thin layer of commercially-available retroreflective paint. Particles within the paint's matrix ensured that a portion of the incident light was returned into the source optical fiber regardless of the belt's finite amplitude or slope. With this technique, vibration measurements were readily made with a strong signal-to-noise ratio, and with a displacement resolution (sub-micron) and bandwidth (DC to 100 kHz) exceeding the test's requirement.

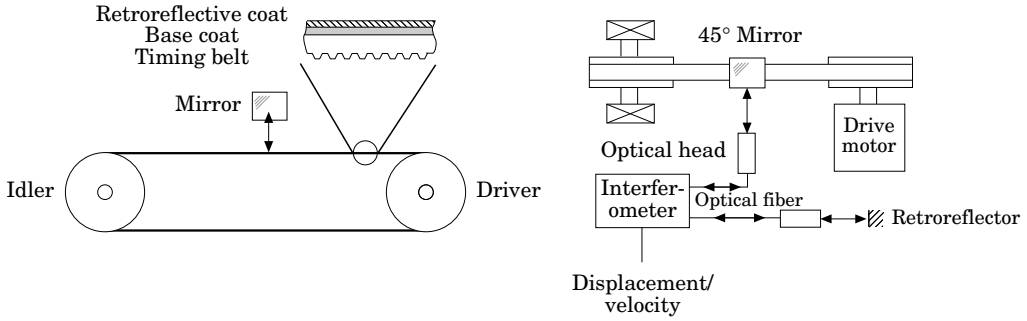

Figure 1. Schematic of the test stand used to measure the vibration of power transmission belts. The timing belt is coated with a retroreflective paint and serves as the target for motion measurement through laser interferometry.

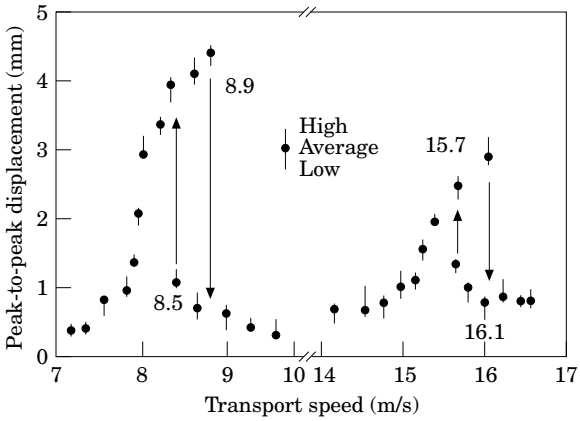

Figure 2. Measured speed-dependent belt response amplitudes over resonance of the first two vibration modes. Data in the non-resonance range 10–14 m/s are omitted for clarity.

An eddy current probe with linear range of approximately 2 mm was used to record the eccentricity of each pulley relative to the rotation axis of its shaft. Measurements were performed on the top lands of the pulley's teeth. Such eccentricity can arise from manufacturing tolerances—particularly so for cast components—and from the clearance between the pulley's hub and shaft which is necessary for assembly. The measured profiles indicated peak-to-peak run-out levels for the drive and idle pulleys of 0·71 and 0·42 mm, respectively, with the maxima being shifted in phase by some 240° of rotation. The relative phase ϕ can be nulled or adjusted to an arbitrary value by proper synchronization of the two pulleys, but in the as-installed condition, ϕ will generally be non-zero.

Measurement of the belt's peak-to-peak response amplitude is shown in Figure 2 as a function of the running speed over $0 < V < 17$ m/s, a range which encompasses resonance of the first two modes. During the tests, the speed was incremented monotonically, and it was then held constant while each amplitude measurement was taken some 1 cm from the driven pulley. Associated with the amplitudes of Figure 2 are the time records of transient response shown in Figure 3, which are obtained as the speed was either increased or decreased through resonance of the fundamental mode near 9 m/s. For instance, when the running speed was increased from 8·4 to 9·2 m/s in Figure 3(a), the amplitude decreased

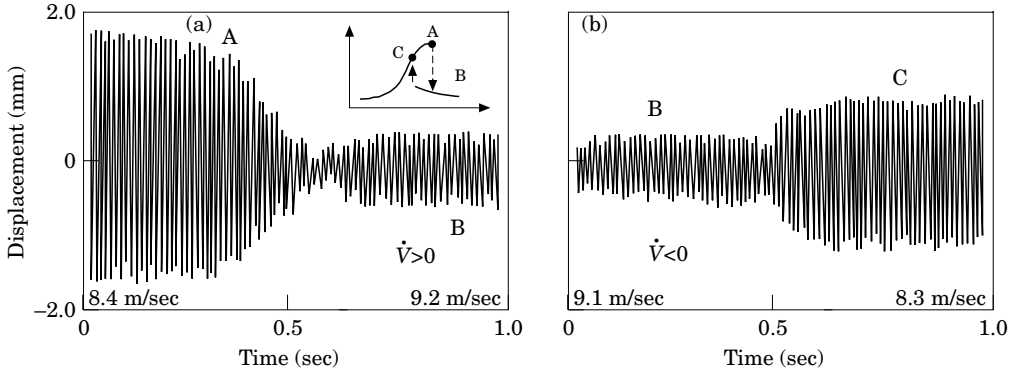

Figure 3. Measured time records depict jumps in amplitude over the first resonance region for monotonically (a) increasing, and (b) decreasing running speeds.

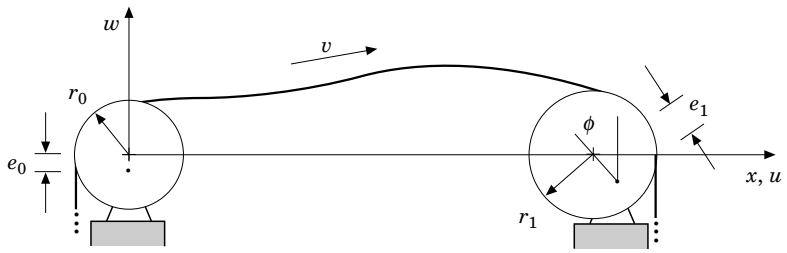

Figure 4. Schematic of the vibration model which comprises a flexible elastic string that is driven by eccentrically-mounted drive and idle pulleys. Quantities r_0, r_1, e_0 and e_1 denote radii and eccentricity.

sharply from the maximal value 1·98 mm to 0·57 mm near $V = 8{\cdot}9$ m/s, as in Figure 2. In the alternative case of Figure 3(b), when the speed was instead decreased through the same range, the amplitude grew from 0·52 mm to 1·51 mm during passage through $V = 8{\cdot}5$ m/s.

Similar non-reversible behavior, in which the vibration amplitude was dual valued and path dependent, was observed at speeds 15·7 m/s and 16·1 m/s, and corresponds to resonance of the belt's second mode. Such classic "jump" behavior is characteristic of a structural non-linearity, and it is attributed here to the longitudinal stretching that occurs as a result of finite amplitude motion in the near-resonance and resonance region.

3. NON-LINEAR VIBRATION MODEL

For the purposes of treating the forced non-linear response, the power transmission belt is idealized as a moving string that is driven harmonically by eccentrically-mounted pulleys. Figure 4 depicts a flexible elastic string that travels under tension P and speed V between the two pulleys identified by the "0" and "1" subscripts. In the light of the belt's measured harmonic natural frequency spectrum, bending stiffness is neglected. The model is further defined by the following assumptions:

Deformation w is confined to the vertical plane, as is suggested by the belt's cross-section being several times wider than it is thick.

Longitudinal deformation u is finite but small when compared with w.

Dynamic responses of the pulleys, power take-offs, and other drive train components are not considered.

Periodic variations of the belt's density ρ and stiffness resulting from joints or teeth are neglected.

In non-dimensionalizing the model, all lengths are measured relative to the span L. The transport speed v is referenced to the speed $v_t = \sqrt{P/\rho A}$ of transverse waves in the belt. With EA denoting the belt's axial stiffness, the longitudinal wave speed $c = \sqrt{E/\rho}$ is several orders of magnitude greater than both V and v_t. For this reason, on the time scales of the lower transverse modes, variations in the belt's tension propagate almost instantaneously, and they can be viewed as being spatially constant to the degree that the influence of longitudinal inertia is small.

At this level of approximation, the longitudinal displacement field is given by

$$u(x, t) = \frac{x}{2}\int_0^1 w_{,x}^2 \, \mathrm{d}x - \frac{1}{2}\int_0^x w_{,x}^2 \, \mathrm{d}x, \tag{1}$$

where the comma-subscript denotes partial differentiation, and it arises entirely from finite w. The equation of transverse motion then becomes [10]

$$w_{,xx} + 2vw_{,xt} + (v^2 - 1)w_{,xx} = \frac{v_l^2}{2} w_{,xx} \int_0^1 w_{,x}^2 \, dx, \tag{2}$$

with solutions being subject to the conditions

$$w(0, t) = e_0 \sin(\Omega_0 t) \qquad \text{and} \qquad w(1, t) = e_1 \sin(\Omega_1 t + \phi) \tag{3}$$

of harmonic motion at the supports. Here e_0 and e_1 denote the dimensionless amplitudes of pulley run-out. In practice, the pulleys can have different radii r_0 and r_1, and so excitation of the belt at the potentially distinct frequencies Ω_0 and Ω_1 is retained in the model. The substitution of transverse displacement w with $w + e_0 \sin(\Omega_0 t) + (e_1 \sin(\Omega_1 t + \phi) - e_0 \sin(\Omega_0 t))x$ renders the boundary conditions (3) homogeneous, and the excitation is transferred in the model from the boundary to the domain. With the definition of the mass, gyroscopic, and linear stiffness operators,

$$M = I, \qquad G = 2v\partial/\partial x, \qquad K = -(1 - v^2)\partial^2/\partial x^2, \tag{4}$$

the non-linear stiffness operator

$$N(w) = \frac{v_l^2}{2} w_{,xx} \int_0^1 w_{,x}^2 \, dx, \tag{5}$$

and the external excitation

$$\begin{aligned} f(x, t) = & -e_0\Omega_0^2 \sin(\Omega_0 t)(1 - x) + \Omega_0 \cos(\Omega_0 t) \\ & - e_1\Omega_1^2 \sin(\Omega_1 t + \phi)x + 2v\Omega_1 \cos(\Omega_1 t + \phi)\Omega_0 \cos(\Omega_0 t), \end{aligned} \tag{6}$$

Equation (2) can be written in the standard symbolic form

$$Mw_{,tt} + Gw_{,t} + Kw = f(x, t) + N(w). \tag{7}$$

Equation (7) is taken as the working form of the belt's equation of motion, which has a particular mathematical structure. Operators M and K are symmetric and positive definite for sub-critical transport speeds, whereas G is skew-symmetric and represents a convective "Coriolis" acceleration component in equation (2).

Power transmission belts are one example of gyroscopic dynamic systems to the degree that their deformation involves small amplitude vibration which is superposed on the mean rigid body motion. Mechanical structures that can vibrate about a state of mean rotation (for instance, disks, shafts, and rotors) or translation (tapes, sheets, and webs) are related by the mathematical similarity of their governing equations of motion [11–13]. In what follows, the perturbation solution which is developed can be applied to any such gyroscopic dynamic system, and to power transmission belts in particular.

4. LINEAR RESPONSE

As the base solution to be used in the perturbation analysis of the belt's non-linear motion, the linear response is first obtained through available closed-form solutions for

the vibration of moving media [11]. In the travelling string model, the Green function is given by

$$g(x, \zeta; t-\tau) = \mathscr{H}(t-\tau) \sum_{n=1}^{\infty} \frac{2}{n\pi} \sin\left(n\pi(1-v^2)(t-\tau) + n\pi v(x-\zeta)\right) \sin(n\pi x) \sin(n\pi\zeta) \tag{8}$$

Although it is represented here in series form, g can in fact be summed exactly with it assuming one of the three values $-1/2$, 0, and $+1/2$. The belt's response to an arbitrary initial displacement w_0, velocity $\dot{w}_0$, and excitation f is then obtained directly through convolution:

$$w = \int_0^1 (\dot{w}_0(\zeta) g(x, \zeta; t) + w_0(\zeta)(g_{,t}(x, \zeta; t) - 2v g_{,\zeta}(x, \zeta; t)))\, \mathrm{d}\zeta$$

$$+ \int_0^t \int_0^1 g(x, \zeta; t-\tau) f(\zeta, \tau)\, \mathrm{d}\zeta\, \mathrm{d}\tau. \tag{9}$$

Following retention of only the steady-state terms in integration, the forced response to excitation (6) becomes

$$\begin{aligned} w(x, t) = & \sum_{n=\pm 1}^{\pm\infty} \frac{e_0 \sin(n\pi x)}{n\pi\omega_n^2(1-\Omega_0/\omega_n)} (\eta_0 \cos(\Omega_0 t - n\pi v(1-x)) \\ & - \cos(n\pi)\{\sin(\Omega_0 t + n\pi v x) + \eta_0 \cos(\Omega_0 t - n\pi v x)\}) \\ & + \sum_{n=\pm 1}^{\pm\infty} \frac{e_1 \sin(n\pi x)}{n\pi\omega_n^2(1-\Omega_1/\omega_n)} (\eta_1 \cos(\Omega_1 t + \phi + n\pi v x) \\ & + \cos(n\pi)\{\sin(\Omega_1 t + \phi - n\pi v(1-x)) + \eta_1 \cos(\Omega_1 t + \phi - n\pi v(1-x))\}. \end{aligned} \tag{10}$$

Here $\eta_0 = 2v(\omega_n - \Omega_0)/\omega_n\Omega_0$, $\eta_1 = 2v(\omega_n - \Omega_1)/\omega_n\Omega_1$, $\omega_n = n\pi(1-v^2)$ for positive n, and $\omega_{-n} = -\omega_n$. In the limit of either $e_0 = 0$ or $e_1 = 0$, the alternative solution of Mahalingam [7] is recovered.

Solution (10) is readily interpreted in terms of the frequency crossing diagram shown in Figure 5, in which the speed-dependent natural and excitation frequencies are monitored as functions of the belt's running speed. The belt's natural frequencies $\omega_n = n\pi(1-v^2)$ decrease quadratically with v, while the synchronous pulley rotation rates grow linearly. In Figure 5, resonance occurs when the load lines $\Omega_0 = Lv/r_0$ and $\Omega_1 = Lv/r_1$, constructed for the left L and right R pulleys, intersect the ω_n loci in a manner analogous to the "Campbell" diagram used in treating the vibration of rotating machinery [6]. The corresponding response amplitude, as predicted by Equation (10), is also shown in Figure 5. The speeds at which resonance occurs are unequally-spaced, a phenomenon which has been observed in the operation of sheet metal rolling mill stacks [14].

5. NON-LINEAR RESPONSE

5.1. ASYMPTOTIC APPROXIMATION

A perturbation solution is developed for a general non-autonomous gyroscopic system with weakly non-linear stiffness and/or dissipation. The present development extends the formulation in reference [10] for the treatment of autonomous gyroscopic systems. In symbolic form, the equation of motion for a non-linear gyroscopic system with monofrequency Ω excitation is written

$$Mw_{,tt} + Gw_{,t} + Kw = \varepsilon f_0(x) \exp(\mathrm{i}\Omega t) + \sum_{n=1}^{N} \varepsilon^n N^{(n)}(w, w_{,t}) + \mathcal{O}(\varepsilon^{N+1}), \tag{11}$$

where $\mathrm{i} = \sqrt{-1}$, in terms of the small amplitude scaling parameter ε. $N^{(n)}$ captures non-linearity caused by large deflection.

Following the averaging method of Krylov, Bogoliubov, and Mitropolsky [15, 16], the solution

$$w(x, t) = w^{(0)}(x; a, \theta) + \sum_{n=1}^{N} \varepsilon^n w^{(n)}(x; a, \theta) + \mathcal{O}(\varepsilon^{N+1}) \tag{12}$$

is developed in the form of a power series in ε, where a and θ are the response's total amplitude and phase. In the non-autonomous case, the difference in phase between the

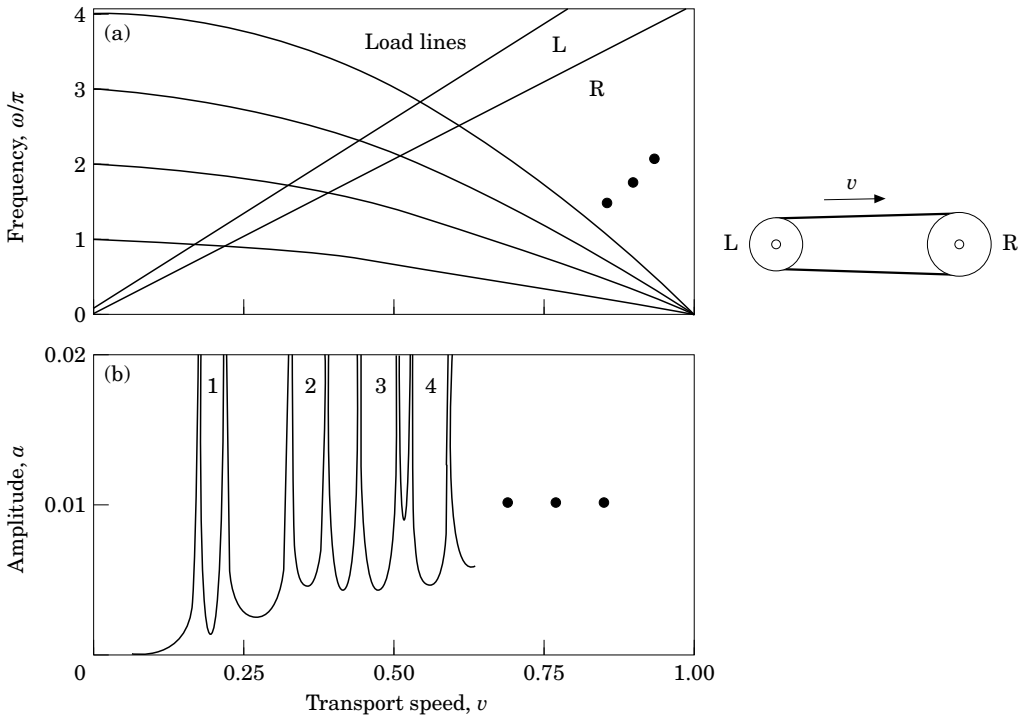

Figure 5. (a) Crossing diagram of natural and excitation frequencies for a belt guided by pulleys with different radii, and (b) the steady-state response amplitude as predicted by equation (10). Intersections of the loci set the speeds at which resonance occurs.

linear natural frequency and the driving frequency influence both a and θ. In this manner, their expansions are taken to be

$$\dot{a} = \sum_{n=1}^{N} \varepsilon^n P_n(a, \varphi) + \mathcal{O}(\varepsilon^{N+1}), \qquad \dot{\varphi} = Q_0 + \sum_{n=1}^{N} \varepsilon^n Q_n(a, \varphi) + \mathcal{O}(\varepsilon^{N+1}). \quad (13, 14)$$

Following substitution into equation (11), the set of equations of motion,

$$\mathcal{O}(\varepsilon^0): \quad \{M((Q_0 D_{,\varphi})^2 + (2Q_0 D_{,\varphi} + D_{,t})D_{,t}) + G(Q_0 D_{,\varphi} + D_{,t}) + K\}w^{(0)} = 0, \quad (15)$$

$$\begin{aligned}\mathcal{O}(\varepsilon^1): \quad & \{M((Q_0 D_{,\varphi})^2 + (2Q_0 D_{,\varphi} + D_{,t})D_{,t}) + G(Q_0 D_{,\varphi} + D_{,t}) + K\}w^{(1)} \\ & = f^{(1)} + f_0(x)\exp(\mathrm{i}\Omega t) - \{M(Q_0(P_{1,\varphi} D_{,a} + Q_{1,\varphi}) + 2P_1(Q_0 D_{,\varphi} + D_{,t})D_{,a} \\ & \quad + 2Q_1(Q_0 D_{,\varphi} + D_{,t})D_{,\varphi}) + G(P_1 D_{,a} + Q_1 D_{,\varphi})\}w^{(0)} \end{aligned} \quad (16)$$

is solved recursively to define the response at successively higher levels of approximation. In equations (15) and (16), $D_{,a} = \partial/\partial a$, $D_{,\varphi} = \partial/\partial\varphi$, $D_{,t} = \partial/\partial t$, and the first-order excitation component

$$f^{(1)} = N(w^{(0)}, (Q_0 D_{,\varphi})w^{(0)}) \quad (17)$$

is evaluated at the known zero-order solution $w^{(0)}$.

In the near- and exact-resonance cases, the phase difference between the response and excitation plays an important role. With $Q_0 = \omega_n - \Omega$, equation (15) is satisfied by the linear single-mode response

$$w^{(0)}(x; a, \varphi) = \tfrac{1}{2} a\psi_n(x)\,\mathrm{e}^{\mathrm{i}\theta} + cc = \tfrac{1}{2} a\psi_n(x)\,\mathrm{e}^{\mathrm{i}(\Omega t + \varphi)} + cc, \quad (18)$$

where cc denotes the complex conjugate of all preceding terms. Equation (18) represents near-resonant motion of the linear belt model in mode ψ_n. The vibration modes are complex, signifying the presence of spatial phase shifts in the free motion of gyroscopic systems, and high speed belts in particular.

At each perturbation level, the non-linear excitation components are represented through their complex Fourier decompositions. In equation (16), for instance,

$$f^{(1)}(x; a, \theta) = \sum_{r=-\infty}^{\infty} f_r^{(1)}(x; a)\,\mathrm{e}^{\mathrm{i}r\theta}, \qquad f_r^{(1)}(x; a) = \frac{1}{2\pi}\int_0^{2\pi} f^{(1)}(x; a, \theta)\,\mathrm{e}^{-\mathrm{i}r\theta}\,\mathrm{d}\theta. \quad (19, 20)$$

In turn, the corrections P_1 and Q_1 in equations (13), (14) are chosen so as to eliminate secular terms that arise in $w^{(1)}$. This requirement leads to the solvability condition

$$\langle f_1^{(1)} + f_0\,\mathrm{e}^{-\mathrm{i}\varphi} - \tfrac{1}{2}((P_1 + \mathrm{i}aQ_1)(G + 2\mathrm{i}\omega_n M) + M(\omega_n - \Omega)(P_{1,\varphi} + \mathrm{i}aQ_{1,\varphi}))\psi_n, \psi_n\rangle = 0, \quad (21)$$

which imposes orthogonality between the excitation's spatial distribution and each particular ψ_n. Here the nomenclature $\langle\cdot, \cdot\rangle$ denotes the standard inner product of two complex functions over $x \in (0, 1)$.

This representation of the solution is simplified when it is written in terms of the real modal mass, gyroscopic, and stiffness constants:

$$m_n = \langle M\psi_n, \psi_n\rangle, \qquad g_n = -\mathrm{i}\langle G\psi_n, \psi_n\rangle, \qquad k_n = \langle K\psi_n, \psi_n\rangle. \quad (22)$$

In this case, the first-order corrections for the response amplitude and phase difference become

$$P_1 = (1/\alpha)\,\mathrm{Im}\,\langle f_1^{(n)}, \psi_n\rangle + (1/\beta)(\mathrm{Im}\,\langle f_0, \psi_n\rangle \cos\varphi - \mathrm{Re}\,\langle f_0, \psi_n\rangle \sin\varphi), \tag{23}$$

$$aQ_1 = (1/\alpha)\,\mathrm{Re}\,\langle f_1^{(n)}, \psi_n\rangle - (1/\beta)(\mathrm{Re}\,\langle f_0, \psi_n\rangle \cos\varphi - \mathrm{Im}\,\langle f_0, \psi_n\rangle \sin\varphi), \tag{24}$$

where α and β are defined as

$$\alpha = \sqrt{m_n}\sqrt{k_n + (g_n/2\sqrt{m_n})} \qquad \text{and} \qquad \beta = (1/2)(-g_n/2 + 3\alpha - m_n\Omega). \tag{25}$$

The equivalent stiffness $\lambda_e^{(1)}$ and frequency $\omega_e^{(1)}$ parameters [15] are then defined by

$$\lambda_e^{(1)} = (\varepsilon/a\alpha)\,\mathrm{Im}\,\langle f_1^{(1)}, \psi_n\rangle, \qquad \omega_e^{(1)} = \omega_n - (\varepsilon/a\alpha)\,\mathrm{Re}\,\langle f_1^{(1)}, \psi_n\rangle, \tag{26, 27}$$

and the amplitude and phase differences are given by the simplified forms

$$\dot{a} = \lambda_e^{(1)}(a)a + (\varepsilon/\beta)\,\mathrm{Im}\,\langle f_0, \psi_1\rangle \cos\varphi - \mathrm{Re}\,\langle f, \psi_1\rangle \sin\varphi \tag{28}$$

$$\dot{\varphi} = \omega_e^{(1)}(a) - \Omega - (\varepsilon/\alpha\beta)\,\mathrm{Re}\,\langle f_0, \psi_1\rangle \cos\varphi - \mathrm{Im}\,\langle f_0, \psi_1\rangle \sin\varphi. \tag{29}$$

The solution (28, 29) for a general gyroscopic system is next specialized to the case of non-linear belt vibration with the model being defined by operators (4) and (5). For the case in which vibration is driven by the eccentricity of the right-hand pulley only, the excitation is expanded:

$$f_0(x)\,\mathrm{e}^{\mathrm{i}\Omega t} = (x - \mathrm{i}2r)\,e_1\Omega^2\,\mathrm{e}^{\mathrm{i}\Omega t} + cc. \tag{30}$$

The response near or at resonance is dominated by mode $\psi_n = \sqrt{2}\sin(n\pi x)\exp(\mathrm{i}n\pi v x)$, which has been normalized in amplitude such that $m_n = 1$. As the belt's running speed grows, so does the imaginary component of ψ_n, which highlights the spatial phase shift that is present in its free or forced vibration. The steady-state response of the belt is defined in terms of the singular points of equations (28) and (29) by the requirements $\dot{a} = \dot{\varphi} = 0$. These stationarity conditions lead to the algebraic equation

$$C_3(a^2)^3 + C_2(a^2)^2 + C_1(a^2) + C_0 = 0 \tag{31}$$

in a^2, where the C_i are time-independent constants obtained by integration; for instance,

$$C_3 = (\varepsilon^2/64)(n\pi)^2(v_l/v)^4 \sin(n\pi v)^6 \cos(n\pi v)^2. \tag{32}$$

The singular points comprise one real and two complex conjugate roots for running speeds below a critical fold velocity v_f, and three real roots above that point. In the case of exact resonance, the so-called "backbone curve" bisects two of the real roots for $v > v_f$ and is defined by

$$\Omega = n\pi(1 - v^2) - \tfrac{1}{8}(\varepsilon a v_l)^2(n\pi)^3((1 + v^2)^2 + \tfrac{1}{2}(\sin(n\pi v)/n\pi v)^2), \tag{33}$$

which can be used to determine at first-order the relation between the exact resonant frequency and the vibration amplitude.

5.2. SINGLE MODE SIMULATION

An alternative solution is developed by discretizing equation (2) and simulating the response through direct numerical integration. In the near- and exact-resonance conditions, the single mode representation

$$w(x, t) = \xi_n^R(t)\psi_n^R(x) + \xi_n^I(t)\psi_n^I(x) \tag{34}$$

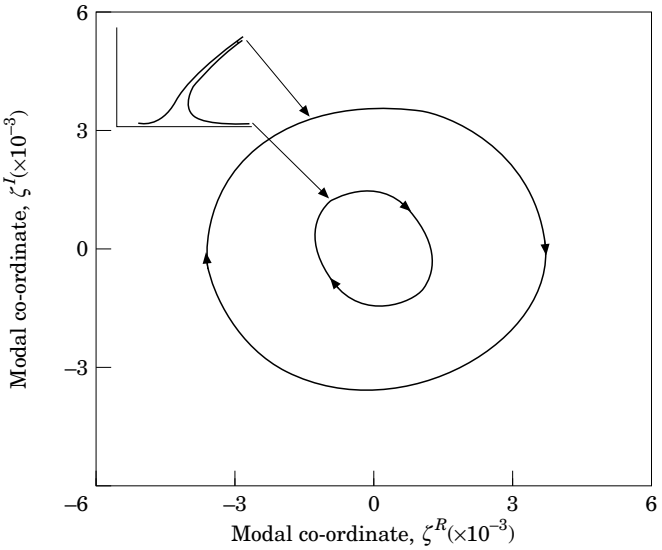

Figure 6. Phase plane trajectories obtained from direct simulation. Taken at identical speeds, the limit cycle amplitudes depend on the chosen initial conditions.

approximates the spatial character of the motion in terms of a specified linear mode, but allows for non-linear temporal behavior. The generalized co-ordinates ξ_n^R and ξ_n^I govern evolution of the real and imaginary components of the eigenfunction ψ_n, as denoted by the superscripts R and I.

Following application of Galerkin's method, the single mode response evolves according to the system

$$\dot{\xi}_n^R - \omega_n \xi_n^I = C_3^R \xi_n^{R3} + C_2^R \xi_n^{R2} \xi_n^I + C_1^R \xi_n^R \xi_n^{I2} + C_0^R \xi_n^{I3} + f_n^R, \tag{35}$$

$$\dot{\xi}_n^I + \omega_n \xi_n^R = C_3^I \xi_n^{I3} + C_2^I \xi_n^R \xi_n^{I2} + C_1^I \xi_n^{R2} \xi_n^I + C_0^I \xi_n^{R3} + f_n^I \tag{36}$$

of first-order ordinary differential equations. The constants C_i^R and C_i^I are determined in closed-form by integration, and f_n^R and f_n^I are the time-dependent excitation components.

To determine steady-state solutions, equations (35), (36) were integrated numerically by using an available fourth/fifth order Runge-Kutta algorithm. In implementation, small numerical modal damping was introduced so as to drive the model to its steady state. While physically realistic, this attribute is not present in the perturbation solution and does restrict some solution comparisons. The double-valued nature of the response amplitude is illustrated in Figure 6, where calculated limit cycle trajectories are shown in the $\xi^R - \xi^I$ state plane. At an identical value of belt's running speed, the steady-state response can assume either of two possible values depending on the trajectory's initial conditions.

The perturbation and simulation solutions are compared in Figure 7 for three different values of the longitudinal stiffness parameter v_l; for the case at hand, $v_l \approx 50$. In the multi-valued response region, the intermediate real root corresponds to a saddle point and therefore a motion which is unrealizable in either numerical or laboratory experiments.

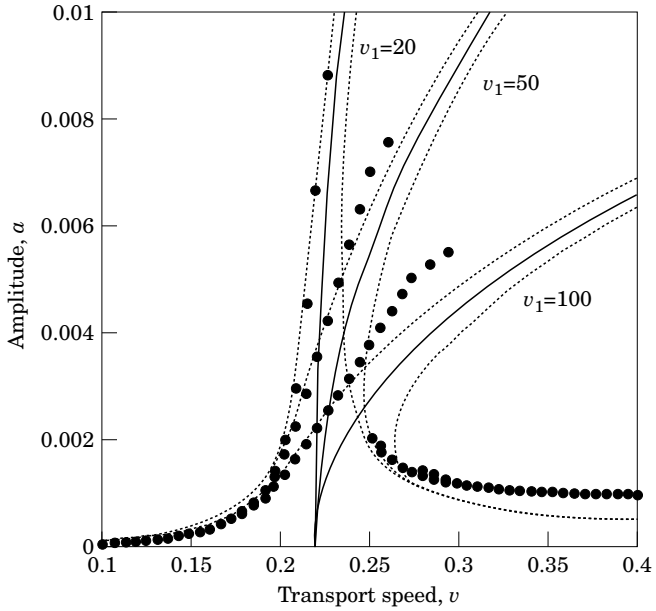

Figure 7. Response amplitudes as predicted by direct simulation (●) and by the closed-form perturbation solution (· · ·). The backbone curve (33) (——) bisects the two branches of the resonance curve.

The remaining two roots, on the other hand, are stable with sensible agreement among the two solutions in Figure 7, and with the measured values in Figure 8. Since the perturbation analysis is based on the premise that the non-linearity is weak, the perturbation solution does become increasingly inaccurate as v_l grows.

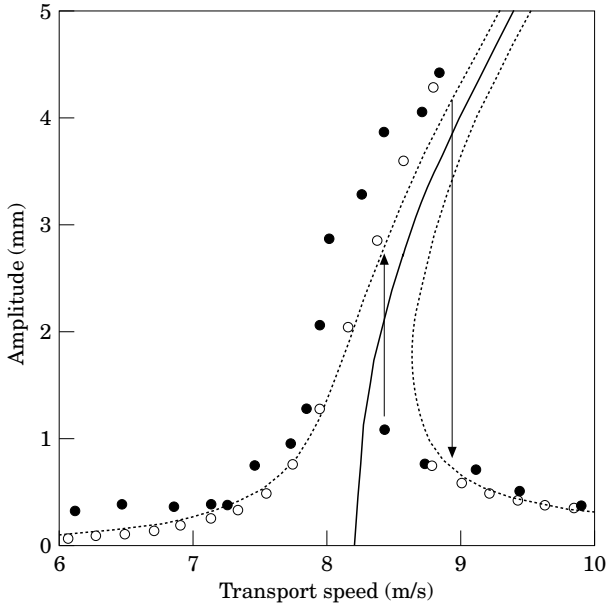

Figure 8. Comparison of the predicted and measured amplitudes in the first resonance region: (●), measured; (○), single mode simulation; and (——) asymptotic solution.

6. SUMMARY

In the case of belt vibration that is driven by pulley or sprocket run-out, both the linear natural frequencies and the excitation frequencies depend on the belt's speed. The former decrease, and the latter increase, with the speed. To that degree, the frequency crossing diagram of Figure 5 can be a useful way to identify the resonance conditions of moving media, analogous to methods for treating the vibration of rotating machine components. The slopes of the load lines are determined only by the ratios of the pulley radii to the belt's span length, and so undesirable designs can be identified graphically.

In the common implementation in which two opposing pulleys have different radii, the belt is subjected to dual-frequency synchronous excitation, with the pattern of resonance speeds as suggested in Figure 5. Other synchronous excitation sources, including meshing teeth on a timing belt, or disturbances arising from the belt seams, can also be incorporated into the frequency crossing diagram.

In the laboratory tests the attendant vibration model, non-linearity manifests itself through dual valued amplitudes and jumps. Inclusion of non-linearity in the near resonance regions is necessary to predict the belt's response with fidelity and explain non-reversible behavior during passage through a resonant speed. In that sense, the perturbation solution is useful for establishing the backbone curve (33) and the relation between speed, resonance, and vibration amplitude. Lacking dissipation, it cannot identify the speed at which an amplitude jump will occur for $\dot{v} > 0$; modal damping can, however, be incorporated into the numerical simulation.

ACKNOWLEDGMENTS

This work was supported by the National Science Foundation and the authors' group of industrial partners.

REFERENCES

1. A. S. Abrate 1992 *Mechanisms and Machine Theory* **27**, 645–659. Vibration of belts and belt drives.
2. J. N. Fawcett and J. S. Burdess 1980 *ASME paper* 800-C2/DET-94. An experimental investigation of the vibration of toothed belts.
3. R. G. S. Gasper and L. E. Hawker 1989 *ASME paper* DE–18, 13–16. Resonance frequency prediction of automotive serpentine belt drive systems by computer modeling.
4. S. Naguleswaran and C. J. H. Williams 1968 *International Journal of Mechanical Sciences* **10,** 239–250. Lateral vibration of band-saw blades, pulley belts, and the like.
5. J. E. Rhodes, Jr. 1970 *ASME Journal of Applied Mechanics* **20**, 1055–1060. Parametric self-excitation of a belt into transverse vibration.
6. A. G. Ulsoy, J. E. Whitesell and M. D. Hooven 1985 *ASME Journal of Vibration*, *Acoustics*, *Stress*, *and Reliability in Design* **107**, 282–290. Design of belt-tensioner systems for dynamic stability.
7. S. Mahalingam 1957 *British Journal of Applied Physics* **8**, 145–148. Transverse vibration of power transmission chains.
8. S. F. Asokanthan and S. T. Ariaratnam 1987 *ASME Journal of Mechanisms*, *Transmissions*, *and Automation in Design* **109**, 412–418. Dynamic stability of chain drives.
9. K. W. Wang 1992 *ASME Journal of Vibration and Acoustics* **114**, 119–126. On the stability of chain drive systems under periodic sprocket oscillation.
10. J. A. Wickert 1990 *International Journal of Non-linear Mechanics* **27**, 503–517. Non-linear vibration of a traveling tensioned beam.
11. J. A. Wickert and C. D. Mote Jr. 1990 *ASME Journal of Applied Mechanics* **57**, 738–744. Classical vibration analysis of axially-moving continua.

12. L. Meirovitch 1975 *ASME Journal of Applied Mechanics* **42**, 446–450. A modal analysis for the response of linear gyroscopic systems.
13. P. C. Hughes and G. M. D'Eleuterio 1986 *ASME Journal of Applied Mechanics* **53**, 919–924. Modal parameter analysis of gyroelastic continua.
14. W. Chan 1995 Personal communication.
15. N. N. Bogoliubov and Y. A. Mitropolsky 1961 *Asymptotic Methods in the Theory of Non-linear Oscillations*. Hindustan Publishing Corporation (translated from Russian).
16. G. N. Bojadziev and R. W. Lardner 1973 *International Journal of Non-linear Mechanics* **8**, 289–302. Monofrequent oscillations in mechanical systems governed by second order hyperbolic differential equations with small non-linearities.